INTERFACE

rsif.royalsocietypublishing.org

Research

Cite this article: Murphy KC, Hung BP, Browne-Bourne S, Zhou D, Yeung J, Genetos DC, Leach JK. 2017 Measurement of oxygen tension within mesenchymal stem cell spheroids. *J. R. Soc. Interface* **14**: 20160851. http://dx.doi.org/10.1098/rsif.2016.0851

Received: 24 October 2016
Accepted: 17 January 2017

Subject Category:
Life Sciences–Engineering interface

Subject Areas:
bioengineering, biomedical engineering

Keywords:
oxygen tension, diffusion, spheroid, hypoxia, mesenchymal stem cell

Author for correspondence:
J. Kent Leach
e-mail: jkleach@ucdavis.edu

Electronic supplementary material is available online at https://dx.doi.org/10.6084/m9.figshare.c.3675931.

THE ROYAL SOCIETY PUBLISHING

Measurement of oxygen tension within mesenchymal stem cell spheroids

Kaitlin C. Murphy[1], Ben P. Hung[1], Stephen Browne-Bourne[1], Dejie Zhou[1], Jessica Yeung[1], Damian C. Genetos[2] and J. Kent Leach[1,3]

[1]Department of Biomedical Engineering, and [2]Department of Anatomy, Physiology, and Cell Biology, School of Veterinary Medicine, University of California, Davis, CA 95616, USA
[3]Department of Orthopaedic Surgery, School of Medicine, University of California, Davis, Sacramento, CA 95817, USA

JKL, 0000-0002-1673-3335

Spheroids formed of mesenchymal stem cells (MSCs) exhibit increased cell survival and trophic factor secretion compared with dissociated MSCs, making them therapeutically advantageous for cell therapy. Presently, there is no consensus for the mechanism of action. Many hypothesize that spheroid formation potentiates cell function by generating a hypoxic core within spheroids of sufficiently large diameters. The purpose of this study was to experimentally determine whether a hypoxic core is generated in MSC spheroids by measuring oxygen tension in aggregates of increasing diameter and correlating oxygen tension values with cell function. MSC spheroids were formed with 15 000, 30 000 or 60 000 cells per spheroid, resulting in radii of 176 ± 8 μm, 251 ± 12 μm and 353 ± 18 μm, respectively. Oxygen tension values coupled with mathematical modelling revealed a gradient that varied less than 10% from the outer diameter within the largest spheroids. Despite the modest radial variance in oxygen tension, cellular metabolism from spheroids significantly decreased as the number of cells and resultant spheroid size increased. This may be due to adaptive reductions in matrix deposition and packing density with increases in spheroid diameter, enabling spheroids to avoid the formation of a hypoxic core. Overall, these data provide evidence that the enhanced function of MSC spheroids is not oxygen mediated.

1. Introduction

Mesenchymal stem cells (MSCs) are under widespread investigation for regenerative therapies [1]. However, a major challenge to the translation of MSC-based therapies into clinical practice is ensuring their survival and function upon transplantation to the defect site [2]. Previous studies have reported that the high death rate and poor engraftment of cells in ischaemic conditions reduces the efficacy of stem cell therapy, as less than 1% of MSCs survive 4 days after transplantation into an ischaemic defect [3]. Possible reasons for these complications include transplantation into a hypoxic and inflammatory environment, as well as loss of extracellular matrix (ECM) produced in culture following proteolytic enzyme treatment commonly used to harvest expanded cells from the culture dish [4,5].

We and others have demonstrated that MSCs exhibit increased overall function and improved survival when formed into three-dimensional spheroids [6–9]. Compared with an equal number of dissociated MSCs, 15 000 cell MSC spheroids exhibited similar caspase 3/7 activity yet secreted up to 100 times the amount of vascular endothelial growth factor. Larger spheroids formed with more MSCs had increased caspase activity coupled with reduced metabolic activity and proliferation [6]. Spheroid size must be carefully considered due to limitations in the diffusive length of nutrient transport, a feature that may render cells in the core of spheroids with radii greater than 200 μm vulnerable to hypoxia and cell death [6]. Some have speculated that the presence of a hypoxic core within the spheroid may pre-programme the cells to promote survival and enhance their trophic factor secretion [10]. Thus, additional advantages may be

conferred by using a spheroid whose radius is near the nutrient transport limitation but not if it is surpassed [11]. Nevertheless, there is disagreement in the literature whether this hypoxic core exists or is necessary for enhanced MSC spheroid function.

Previous studies using cancer cells and hepatocytes have used oxygen-sensitive microelectrodes to measure their steady-state oxygen values [12–14], while others generated predictive mathematical models but were unable to directly measure oxygen tension values for model validation [11]. Although numerous modelling studies have been devoted to the investigation of transport phenomena throughout spheroids [11,15–17], previous studies were conducted with non-MSC populations that consume oxygen and nutrients at different rates [18]. Additionally, the significance of spheroid formation for MSCs is vastly different from cancer cells and hepatocytes, as MSCs do not naturally form spheroid-like bodies *in vivo* but are instead used as a tool to prime the cells for maximum trophic factor secretion [7]. Lastly, the packing density and porosity would differ between cell types, causing the rate of diffusion to differ [19].

The purpose of this study was to evaluate the oxygen tension profile in MSC spheroids to establish the existence of a hypoxic core and subsequently correlate cell survival with oxygen availability in these aggregates. We used an oxygen-sensitive microelectrode to measure oxygen tension as a function of radius within spheroids of increasing diameters. Data were used to numerically describe oxygen gradients within spheroids using a mathematical model. We measured cell viability and metabolism as a function of spheroid size. Finally, we measured spheroid diameter and packing density to examine a potential pathway of cell survival in larger spheroids. The results of these studies offer an enhanced understanding of the interplay among spheroid size, nutrient transport and cell function.

2. Material and methods

2.1. Cell culture

Human bone marrow-derived MSCs (Lonza, Walkersville, MD) from two donors were used without additional characterization. MSCs were expanded in standard culture conditions (37°C, 21% O_2, 5% CO_2) in minimal essential medium–alpha modification (α-MEM) supplemented with 10% fetal bovine serum (Atlanta Biologicals, Flowery Branch, GA) and 1% penicillin/streptomycin (P/S; Gemini, Sacramento, CA) until use at passages 4–5.

2.2. Spheroid formation and characterization

MSC spheroids were formed using the hanging drop technique over 48 h with 15 000, 30 000 or 60 000 cells per 25 µl droplet [6]. This range was selected due to previous reports of resulting sizes below and above the diffusion limit of oxygen, known increases in trophic factor secretion, and to examine spheroids of similar sizes reported in the literature [9,20,21]. This formation duration was selected due to its ability to consistently form tightly packed spheroids [21]. After the spheroids had aggregated for 48 h, spheroid diameter was quantified via bright field microscopy and analysed with ImageJ (NIH, Bethesda, MD).

2.3. Oxygen tension measurements

Oxygen tension within the spheroid was measured in ambient air at 25°C using a Unisense oxygen microsensor OX-10 with an outside tip diameter of 10 µm and detection limit of 0.3 µM O_2 (Unisense, Aarhus N, Denmark). Spheroids were held under weak aspiration by a glass micropipette, and microsensor placement was visualized using an Eclipse TS100 microscope (Nikon, Melville, NY). The focal plane was used to place the microsensor in the middle of the spheroid, and oxygen tension measurements were taken every 10 µm until the centre of the spheroid. The entire diameter of the spheroid was not profiled to avoid contact between the microsensor and the glass micropipette (figure 1*a*).

2.4. Mathematical modelling

After oxygen tensions at the corresponding positions were sampled, these data were used to generate a mathematical model. As the MSCs within the spheroids are consuming oxygen as it diffuses to the centre, we fitted the data to the mass transfer equation for diffusive transport with simultaneous consumption as previously described [12,13]:

$$\frac{\partial C}{\partial t} = D\nabla^2 C - \psi, \tag{2.1}$$

where C is the concentration of oxygen; t is time; D is the binary diffusion coefficient; and ψ is the reaction term using the following assumptions:

(i) The system was at steady state.
(ii) Changes in O_2 occurred only in one dimension, the radial coordinate r, and did not depend on the polar (θ) or the azimuthal (φ) angles.
(iii) The reaction rate of oxygen consumption was a zero-order reaction; the cells are consuming oxygen at a maximum rate K that is constant within each spheroid [17].

The equation can be rewritten in terms of the spherical Laplacian as

$$\frac{K}{D} = \frac{1}{r^2}\frac{\partial}{\partial r}\left(r^2\frac{\partial C}{\partial r}\right), \tag{2.2}$$

where r is the radial coordinate.

The differential equation can then be written as

$$\frac{K}{D} = \frac{\mathrm{d}^2 C}{\mathrm{d}r^2} + \frac{2}{r}\frac{\mathrm{d}C}{\mathrm{d}r}. \tag{2.3}$$

And the applicable solution is

$$C_0 - C(r) = \frac{K}{3D}\left[\frac{R^2 - r^2}{2} + \frac{b^3}{R} - \frac{b^3}{r}\right], \tag{2.4}$$

where R is the spheroid radius; C_0 is the concentration of oxygen at the spheroid surface; and b is the radius at which $\mathrm{d}C/\mathrm{d}r = 0$, which represents the boundary of the hypoxic core within the spheroid (figure 1*b*,*c*) [12].

This can be further simplified to

$$C_0 - C(r) = \alpha - \beta r^2 - \frac{\gamma}{r}, \tag{2.5}$$

where

$$\alpha = \frac{K}{3D}\left[\frac{R^2}{2} + \frac{b^3}{R}\right],$$

$$\beta = \frac{K}{6D}$$

and

$$\gamma = \frac{Kb^3}{3D}.$$

To solve for K/D [=]mol/(L * cm^2) and b[=]µm, the concentration of oxygen and the corresponding radial position within the spheroid were inputted into equation (2.5) and integrated numerically in MATLAB (Mathworks, Natick, MA).

2.5. Analysis of spheroid size and packing density

To estimate the spheroid radius, cell assembly into spheroids was assumed to follow the behaviour of close packing of uniform hard spheres. The maximal volume fraction attainable by

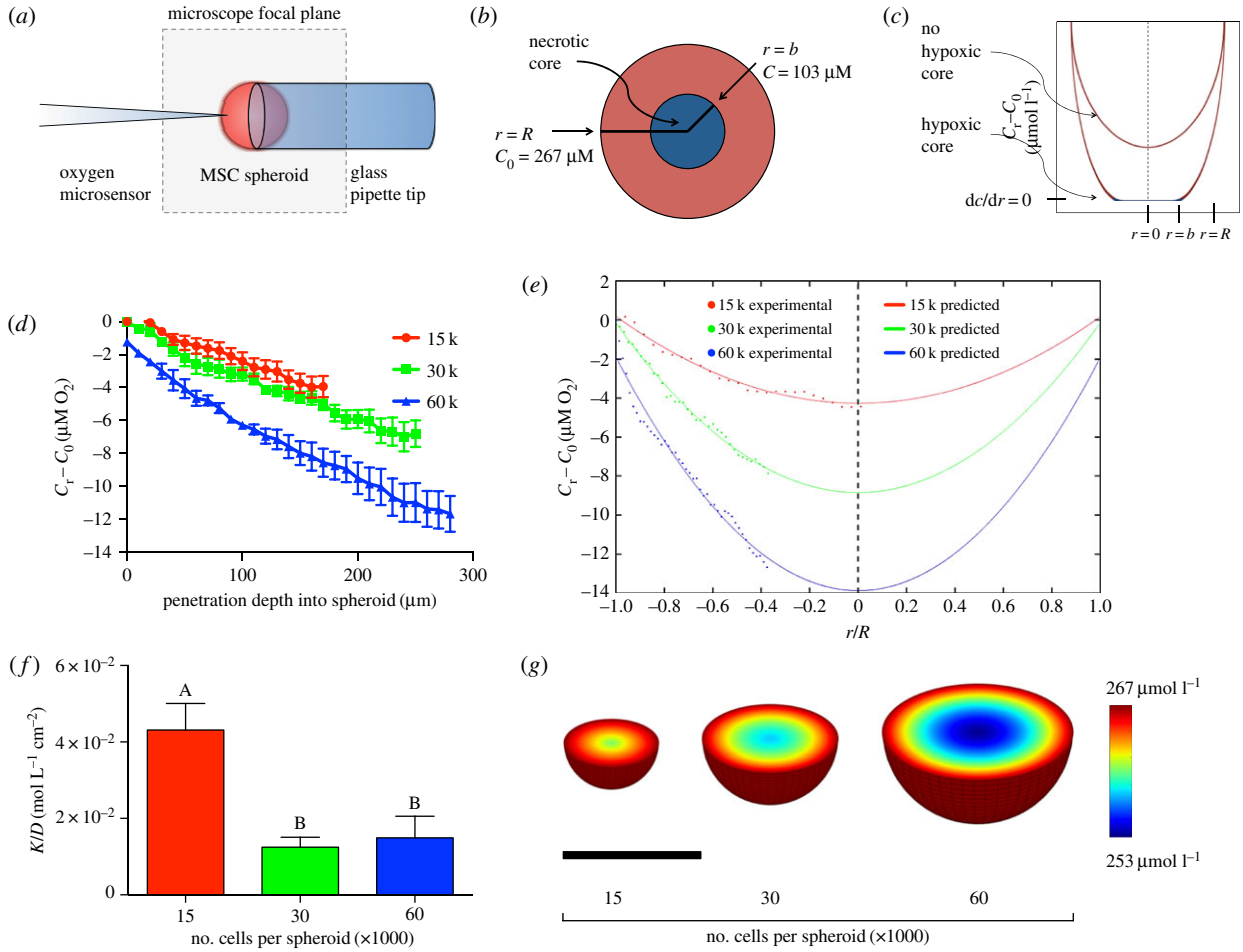

Figure 1. Numerical prediction of oxygen tension within MSC spheroids. (*a*) Experimental set-up of the oxygen microsensor and MSC spheroid; (*b*) diagram demonstrating the presence/absence of a hypoxic core; (*c*) theoretical schematic demonstrating the effect of the presence/absence of a hypoxic core on the oxygen tension profile; (*d*) measured oxygen tension values as a function of distance into the spheroid ($n = 5$). (*e*) Using the measured oxygen tension values, a mathematical model was generated from the averaged data for each spheroid size using equation (2.5) and was plotted alongside the averaged oxygen tension values at each point within the spheroid. (*f*) *K*/*D* was calculated for each spheroid from the measured oxygen tension values ($n = 5$). (*g*) Oxygen tension as a function of radius was visualized in the three-dimensional space by mapping the mathematical model over the cross section of a sphere of the appropriate diameter. Scale bar represents 250 µm. Groups with no significance are linked by the same letters, while groups with significance do not share the same letters.

arrays of similarly sized hard spheres is $\pi/3\sqrt{2} \cong 0.74$, and the diameter of MSCs within the spheroid was estimated to be 15 µm [22], resulting in a volume of 1767 µm^3 per MSC.

$$\text{Predicted spheroid radius} = \sqrt[3]{\left\{\frac{3}{4\pi}\right\}\text{no. of cells per spheroid} \times \text{volume of MSC} \times 0.74}. \quad (2.6)$$

The packing densities were calculated using known cell numbers divided by the aggregate volume, assuming a spherical shape.

$$\text{Packing density } [=]\text{cells cm}^{-3} = \frac{\text{no. of cells per spheroid}}{4/3\pi R^3}. \quad (2.7)$$

2.6. Assessment of cellular function

After spheroid formation, MSCs were lysed in passive lysis buffer (Promega, Madison, WI) and apoptosis was quantitatively measured by analysing 100 µl lysate per sample by using a Caspase-Glo 3/7 assay (Promega) [6,9]. Luminescence was detected on a microplate reader and normalized to DNA content, which was determined from the same lysate by using the Quant-iT PicoGreen DNA Assay Kit (Invitrogen, Carlsbad, CA). Protein concentration was determined using the bicinchoninic acid assay (Thermo Fisher Scientific, Rockford, IL) according to the manufacturer's instructions and normalized to DNA content. Glucose and lactate concentrations were determined from media samples and the lysis buffer, and concentration was assessed using colorimetric assay kits according to the manufacturer's protocols (Abcam, Cambridge, MA) [11]. The glucose consumption was calculated by subtracting the remaining concentration of glucose from the initial stock medium as reported by the manufacturer, 5.5 mM (Invitrogen) [23,24]. As there is no lactate present in α-MEM, all lactate measured in the media was calculated as a product of cellular respiration. Glucose-6-phosphate (G6P) was assessed from the lysate using a commercially available enzymatic assay (Sigma-Aldrich, St Louis, MO) as per the manufacturer's instructions and normalized to cell number.

2.7. Histological analysis

Cell viability of MSC spheroids was assessed by a live–dead assay (Invitrogen) based on the simultaneous determination of live and dead cells with calcein AM and propidium iodide [9]. As a positive control for propidium iodide, spheroids containing 60 000 cells per spheroid were incubated in 70% methanol prior to incubation with the calcein AM/propidium iodide solution for 30 min as per the manufacturer's instructions. To visualize regions of apoptosis within spheroids at early to

intermediate stages of apoptosis [25,26], annexin V conjugated to fluorescein isothiocyanate (FITC) (Thermo Fisher Scientific) was applied to sections at a dilution of 1 : 20 within a buffer composed of 10 mM 4-(2-hydroxyethyl)-1-piperazineethanesulfonic acid, 140 mM sodium chloride and 2.5 mM calcium chloride. Samples were incubated with annexin V for 30 min at 37°C prior to washing and imaging. Viable cells determined by trypan blue exclusion served as a negative control for annexin V staining, while cells incubated in 750 nM staurosporine for 20 h [27], along with 500 000 cell spheroids, served as a positive control. All samples were treated using 4′,6-diamidino-2-phenylindole (DAPI) nuclear counterstain. The area of FITC signal (annexin V) was normalized to the area of blue signal (cell nuclei) to determine an apoptotic index for the inner and peripheral regions of each spheroid, thereby indicating whether an apoptotic core existed within the spheroids.

To visualize regions of hypoxia within the spheroids, pimonidazole hydrochloride (200 µM; Hypoxyprobe; Chemicon, Temecula, CA) was added to the spheroids and incubated in ambient air for 2 h. As a positive control, spheroids containing 60 000 cells per spheroid were incubated in 1% oxygen for 5 days prior to collection, where incubation with pimonidazole also occurred in 1% oxygen [28]. Primary detection was performed with a 1 : 50 dilution of the mouse monoclonal anti-pimonidazole IgG included in the kit, and cells were counterstained with DAPI.

Spheroids were imaged using an Eclipse TE2000U microscope (Nikon, Melville, NY) and an Andor Zyla digital camera (Oxford Instruments, Abingdon, UK). Spheroids were collected and fixed in 10% formalin, washed with phosphate-buffered saline, and then embedded in HistoGel (Richard-Allan Scientific, Kalamazoo, MI). Samples were embedded in Tissue-Tek OCT compound (Sakura, Torrance, CA), and 10 µm sections were cut on a CM1850 Cryostat (Leica Microsystems, Bannockburn, IL) and mounted onto microscope slides (VWR Superfrost Plus Micro Slide; VWR International, Radnor, PA) for analysis. To visualize cell morphology, spheroids were collected and cryosectioned as described above yet with no staining prior to collection. Sections were then stained with H&E and imaged.

2.8. Statistical analysis

Data are presented as mean ± s.d. of the mean. Statistical analysis was performed using a one-way ANOVA with either Tukey's post hoc correction for multiple comparisons or paired *t*-tests when appropriate. All statistical analyses were performed in PRISM. v. 7 software (GraphPad, San Diego, CA); *p*-values of less than 0.05 were considered statistically significant. Significance is denoted by alphabetical lettering; groups with no significance are linked by the same letters, while groups with significance do not share the same letters.

3. Results

3.1. Numerical simulation of oxygen profiles in mesenchymal stem cell spheroids

Oxygen tension was measured every 10 µm for spheroids of different sizes (figure 1*d*). Oxygen tension in the culture medium was experimentally measured as 267 µM O_2, which was constant among spheroids of different sizes. Spheroids were transferred from their hanging droplet to the microscope slide just prior to analysis. The gradient in oxygen tension was not significantly different between 15 000- and 30 000-cell spheroids, whereas the rate at which the oxygen tension decreased in the 60 000-cell spheroid was nearly twice that of the 15 000- and 30 000-cell spheroids. Data were normalized into the non-dimensional unit r/R, and from these experimental data, a mathematical model was generated for each spheroid using equation (2.5) (figure 1*e*). The α, β and γ values were calculated for each spheroid, which were then used to calculate b and K/D. For all three spheroid sizes, we determined that $\gamma \cong 0$, indicating $b = 0$. In these studies, we defined hypoxia as the critical oxygen tension that would permit cell viability and function. If cells were no longer viable, then they would not be able to consume oxygen and nutrients, thus the b-value represents the boundary of the hypoxic core where $dC/dr = 0$. Therefore, since $b = 0$ for these MSC spheroids, these findings suggest that a hypoxic core does not exist within these spheroids.

While a gradient clearly exists within the spheroids that expectedly increases with increasing spheroid size, the largest spheroid containing 60 000 cells per spheroid exhibits less than a 10% decrease in oxygen tension between the outer layer of cells and the inner core. Regardless of spheroid diameter, the oxygen tension values do not approach a point at which $dC/dr = 0$ prior to the centre point, indicating that these spheroids do not exhibit a limitation for the mass transfer of oxygen. The α and β coefficients from the mathematical model were then used to calculate K/D for each spheroid. The smallest spheroids (15 000 cells per spheroid) exhibited increased K/D values compared with the other two sizes, indicative of a smaller diffusion coefficient if the reaction rate of oxygen consumption is assumed to be constant within spheroids of differing diameters (figure 1*f*). This assumption was verified by numerically solving for K/D at each point using equation (2.4) (data not shown). To visualize the oxygen gradient in three dimensions, numerical data were mapped over the cross section at the midplane of the sphere, varying the diameter of the sphere to that of the average spheroid diameter for each size (figure 1*g*).

3.2. Packing density decreases with increasing spheroid size

We noted that the measured radii did not follow a cubic relationship with the number of cells per spheroid. To visualize this, the predicted spheroid radius, assuming maximal packing density, was calculated using equation (2.6) and plotted with the measured radii (figure 2*a*). The measured radii of the smaller spheroids (15 000 cells per spheroid) correlated well with the predicted radii, yet the 30 000- and 60 000-cell spheroids were 16% and 25% larger than their corresponding predicted radii, respectively. From these data, it became evident that the packing density of the MSC spheroids must decrease as the spheroid size increased, allowing oxygen and nutrients to penetrate more easily into the centre of the spheroid. Thus, the packing density was calculated using equation (2.7), and we confirmed that as the number of cells per spheroid increased the cells significantly decreased their packing density within the spheroid (figure 2*b*). To verify that differences in spheroid diameter were due to packing density and not cell proliferation, we quantified the DNA content as an indicator of cell number within each spheroid. DNA content correlated with the number of cells per spheroid ($R^2 = 0.964$), confirming that all MSCs per droplet were incorporating into the spheroids and there was no increase in cell number during spheroid formation (figure 2*c*). Protein content per cell decreased as packing density decreased (figure 2*d*), suggesting relative

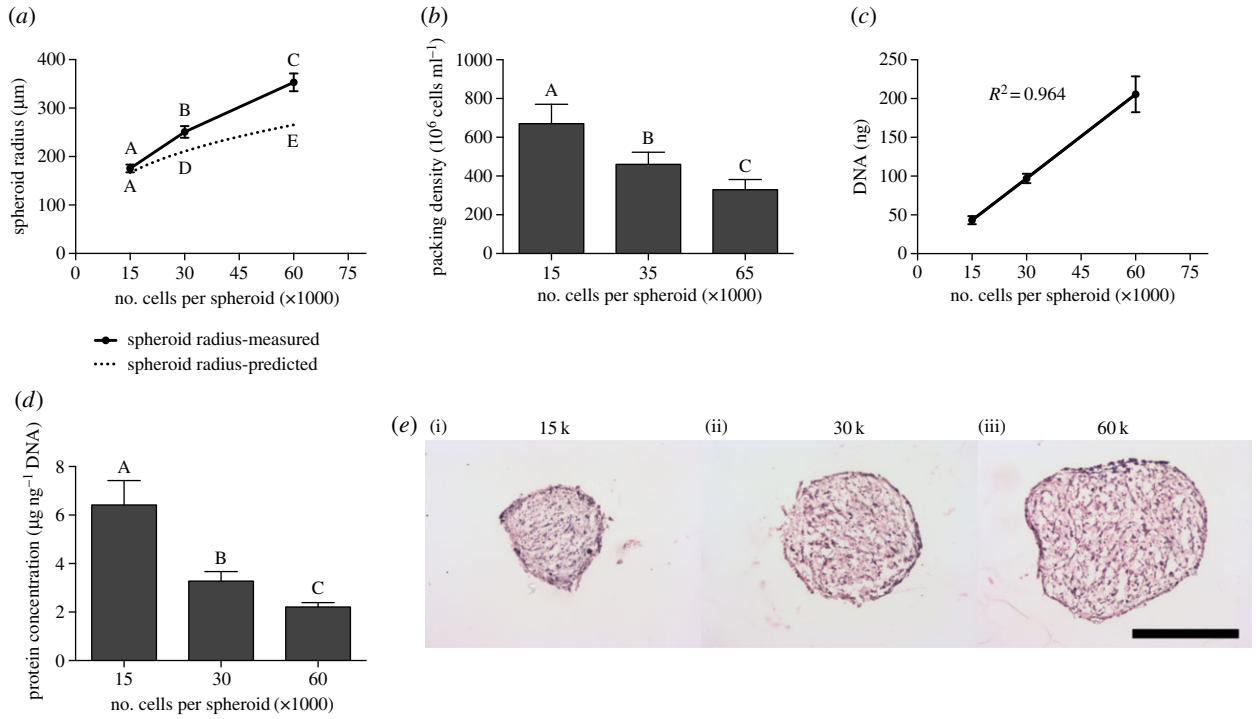

Figure 2. Spheroid packing density decreases as spheroid size increases. (*a*) The predicted spheroid radius assuming maximal packing density was calculated and reported with the measured spheroid radii ($n = 5$). (*b*) As spheroid size increases, the packing density significantly decreases ($n = 5$). (*c*) DNA content increases linearly with the number of cells per spheroid ($n = 3$ per biological donor). (*d*) Normalized protein content decreases with increasing spheroid size ($n = 3$ per biological donor). (*e*) H&E staining indicates that the 15 000-cell spheroids (i) are more compact than the larger 30 000-cell (ii) and 60 000-cell spheroids (iii). Scale bar represents 250 μm. Groups with no significance are linked by the same letters, while groups with significance do not share the same letters. (Online version in colour.)

decreases in ECM content within larger spheroids. Cell packing density and ECM content were further visualized using haematoxylin and eosin (H&E), and numerous cavities throughout the spheroid structure became more evident with increasing spheroid size. H&E staining also revealed that the outer layer of cells appeared more densely packed and elongated than the interior of the spheroid for all three sizes, and spheroids generally became less spherical as diameter increased (figure 2*e*).

3.3. Cell viability and metabolic activity decreases with increasing spheroid size

The largest spheroids (60 000 cells per spheroid) exhibited increased caspase activity, indicative of apoptosis, compared with the smaller 15 000- and 30 000-cell spheroids (figure 3*a*). The aerobic state of spheroids was investigated by measuring glucose consumption and lactate production. Total glucose consumption significantly decreased with increasing spheroid size, with the 15 000-cell spheroids consuming approximately fourfold more glucose than the larger 60 000-cell spheroids (figure 3*b*). Larger spheroids consumed less glucose than their smaller counterparts, as evidenced by measurement of intracellular glucose and glucose-6-phosphate levels (electronic supplementary material, figure S1*a*,*b*). Intracellular glucose measures instantaneous levels compared with the total glucose consumption over 2 days, thus motivating the order-of-magnitude reductions from total glucose consumption. Total L-lactate production followed the same trend as glucose consumption (figure 3*c*). As no L-lactate is present in α-MEM, all L-lactate was a result of cellular metabolism. The yield of lactate from glucose was similar for all groups, regardless of spheroid size (electronic supplementary material, figure S1*c*).

3.4. Histological detection of cell viability and hypoxia

Cell viability within spheroids was visualized using live/dead dyes, revealing no discernable differences between spheroids of different sizes. The absence of dead cells within the larger spheroids was further validated by comparing the spheroids with a positive control, in which spheroids containing 60 000 cells per spheroid were incubated in 70% methanol in order to kill the cells prior to incubation with the live/dead dye (figure 4*a*). From these images, it is evident that cells within each spheroid size are alive and viable. The methanol solution caused the spheroids in the positive control group to contract, leading to an oblong shape. Annexin V staining further confirmed the absence of apoptotic cells within the core of spheroids of 15 000, 30 000 and 60 000 cells (figure 4*b*,*c*). These results differ slightly from our data quantifying caspase 3/7 activity, which is indicative of cells actively undergoing apoptosis. Caspase activity is highly sensitive and measured as relative luminescence, making it is more valuable for comparing within samples than for asserting the presence or the absence of apoptosis since all cell populations have a baseline of apoptotic activity.

Immunohistochemical staining further validated our oxygen tension measurements and verified the absence of a hypoxic core, as there was no pimonidazole staining within any of the spheroids (figure 5). Pimonidazole fluorescently labels regions below 14 μM O_2 and is commonly used in cancer cell spheroids as well as hepatocyte spheroids to demarcate the boundary of the hypoxic core [17,29]. Thus, the absence of a fluorescent signal indicates that a hypoxic core does not exist within these spheroids. The positive control (60 000 cells per spheroid incubated in 1% O_2 for 5 days prior to collection) yielded looser, smaller spheroids, possibly due to a high degree of cell death as the medium was not refreshed.

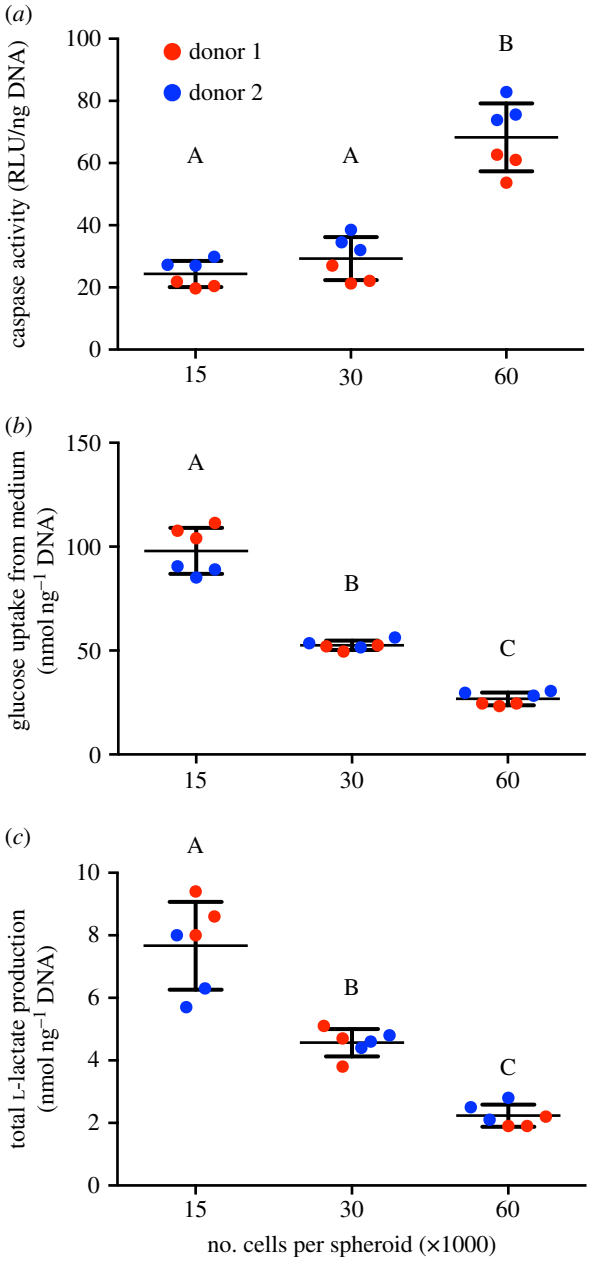

Figure 3. Cell survival and glucose consumption is affected by spheroid size. (*a*) Caspase 3/7 activity in MSC spheroids, (*b*) total glucose consumption and (*c*) total L-lactate production. For all data, $n = 3$ per biological donor. Groups with no significance are linked by the same letters, while groups with significance do not share the same letters. (Online version in colour.)

To determine whether spheroids of larger diameters would exhibit significant apoptosis and hypoxia within their cores, spheroids of 100 000, 250 000 and 500 000 cells were formed and subjected to both annexin V and pimonidazole staining. In contrast to the results reported here for 15 000-, 30 000- and 60 000-cell spheroids, a statistically significant hypoxic core was observed beginning from a size of 250 000 cells per spheroid (electronic supplementary material, figure S2), which correlated with a significant annexin V signal in the core (electronic supplementary material, figure S3). These results indicate that hypoxic cores within MSC spheroids do exist and correlate with increased apoptosis, but only at much larger sizes than those studied here.

4. Discussion

MSC spheroids exhibit increased cell survival and trophic factor secretion compared with individual cells, making them a promising alternative for transplantation in cell-based therapies. However, there is disagreement in the literature whether MSC spheroids contain a hypoxic core and if this hypoxic core is directly responsible for these enhanced properties [7,30–33]. In these studies, we determined that the oxygen gradient within MSC spheroids varied less than 10% from bulk, external oxygen tensions. As MSC spheroid size increased, the packing density within the spheroids decreased, thus facilitating oxygen and nutrient transport. Nonetheless, we determined that glucose consumption was markedly altered with increasing spheroid size. These data demonstrate that MSC spheroid function is modulated with spheroid size, yet this enhanced function of MSC spheroids is not due to a hypoxic core.

The assumed presence of a hypoxic core within MSC spheroids is largely based on reports demonstrating hypoxic and necrotic cores within spheroids formed of cancer cells, and, more recently, hypoxic cores within hepatocyte spheroids [11–13,17,34]. One cannot translate these findings to MSCs, as both cancer cells [35] and hepatocytes [36] reside in highly oxygenated niches, while MSCs typically reside in niches with much lower physiological oxygen tensions [37]. Thus, the oxygen tensions capable of inducing necrosis may be different between cell types. Furthermore, the application of MSC spheroids is vastly different from cancer spheroids, as spheroid formation primes MSCs for increased trophic factor secretion, while cancer spheroids are used as *in vitro* tumour models. Because of the radiation-resistant nature of hypoxic tumours, cancer spheroids are designed to exhibit a necrotic core surrounded by a hypoxic region to effectively examine treatment strategies [38,39]. While we did not detect a hypoxic core in spheroids formed with 60 000 MSCs or fewer, others reported stabilization of hypoxia-inducible factor (HIF-1α) within MSC spheroids, representing a potential pathway for improved cell survival and growth factor secretion [40]. However, this claim was based upon immunofluorescent staining of MSC spheroids less than 200 µm in diameter, and the staining occurred exclusively at the spheroid periphery, more likely the result of aggregation stress than an oxygen tension gradient. Others have investigated the presence of a hypoxic core through histological analysis of spheroid cross sections and demonstrated proliferating cells in spheroids up to 1000 µm in diameter [6,41,42]. To our knowledge, this is the first study to directly measure spatial distribution of oxygen tension within MSC spheroids, which did not approach hypoxic conditions in the centre of even the largest spheroids formed from 60 000 MSCs. In fact, we did not detect the formation of a hypoxic core until making spheroids containing at least 250 000 MSCs. Hypoxia does not have a strict definition in terms of oxygen tension and is dependent on cell type and physiological conditions. We defined hypoxia as the critical oxygen tension that would permit cell viability and function. We observed only small changes in oxygen tension experimentally and numerically, which were insufficient to induce signs of cellular distress via histological analysis, indicating that hypoxic signalling was not occurring within these spheroids. However, due to equipment limitations, these studies were performed in ambient air and the induced gradient may become more significant *in vivo* where oxygen and nutrients are less available. Nonetheless, this does not diminish the impact of these findings, as the increase in trophic factor secretion by MSC spheroids in ambient conditions has been previously reported [9,21,43].

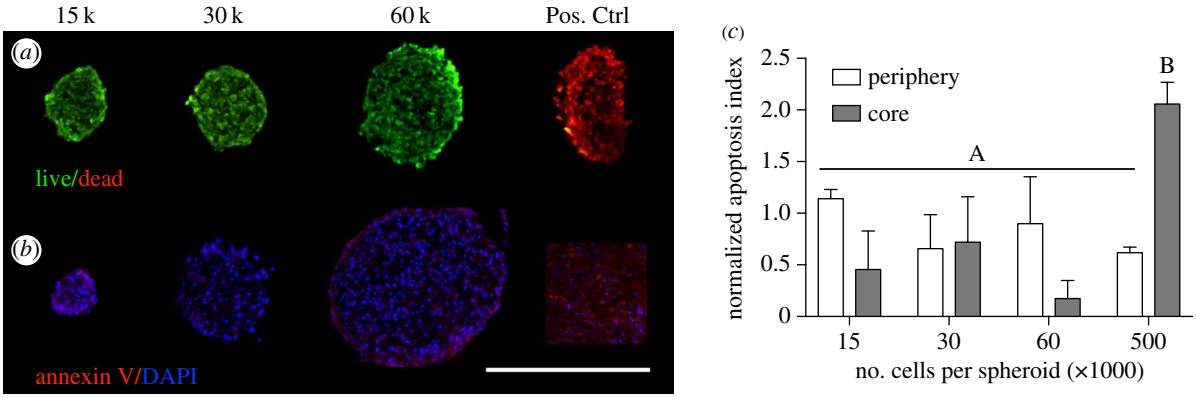

Figure 4. Histological analysis of cell viability revealed no significant differences between spheroids of different diameters. (*a*) Live (green)/dead (red) staining revealed that MSCs in the 15 000-, 30 000- and 60 000-cell spheroids are equally viable. A 60 000-cell spheroid was incubated in methanol as a positive control for propidium iodide (far right). (*b*) Annexin V (red) and DAPI (blue) staining further verified the absence of apoptosis, as the 15 000-, 30 000- and 60 000-cell spheroids did not stain positively in either the spheroid core or the periphery. A 500 000-cell spheroid served as a positive control for Annexin V. Scale bar represents 500 μm; images were captured using a 20× objective. (*c*) Quantification of apoptotic index, calculated by the area of positive Annexin V staining in the core relative to the periphery ($n = 3$). Groups with no significance are linked by the same letters, while groups with significance do not share the same letters.

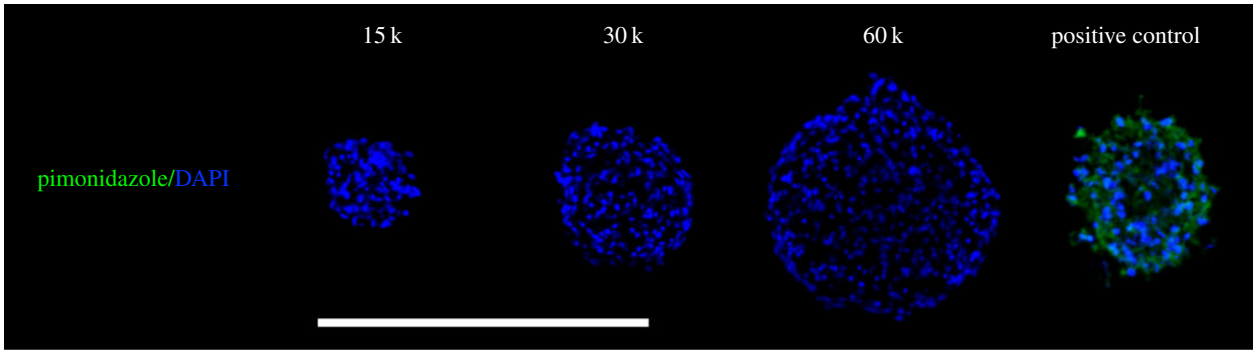

Figure 5. Histological analysis of hypoxia revealed no significant differences between spheroids of different diameters. Pimonidazole (green) and DAPI (blue) staining further verified the absence of a hypoxic core in the 15 000-, 30 000- and 60 000-cell spheroid. A 60 000-cell spheroid was incubated in 1% oxygen for 5 days as a positive control for pimonidazole staining (right). Scale bar represents 500 μm; images were captured using a 20× objective.

As the number of cells per spheroid increased, the packing density decreased, resulting in tightly packed, smaller spheroids and loosely packed, larger spheroids. This may account for why oxygen tension was not significantly reduced in the larger spheroids, as the greater intercellular space allowed for the transport of oxygen and nutrients to the centre of the spheroid. Studies in spheroids of select cancer lines [44] failed to demonstrate such a correlation between spheroid size and packing density [45,46]. While cell viability and actin-mediated contractility were positively correlated in MSC spheroids [47], this adaptive packing density has not been previously reported with spheroids formed of this population. However, differences in MSC spheroid morphology have been noted due to differentiation state [41,48] and dynamic culture conditions [49], both of which could affect oxygen diffusion throughout the spheroid. The increase in oxygen diffusivity is also reflected in the K/D values, as the smaller, tighter packed spheroid containing 15 000 cells per spheroid exhibits a K/D value more than double that of the 60 000 cell spheroids. Interestingly, although the oxygen gradient was not severe, increasing the number of cells per spheroid significantly increased caspase activity and decreased metabolic activity. This is in agreement with our previous study in which we found that smaller spheroids had greater metabolic activity and proliferation [6]. Others have reported that changing the number of cells per spheroid had no effect on adenosine triphosphate (ATP) levels on a per cell basis; however, those studies were performed with spheroids ranging from 500 to 5000 cells per spheroid that may not have been sufficiently large enough to induce changes in metabolic activity [47].

Numerous studies have reported increased caspase activity in MSC spheroids, and it has been postulated that this phenomenon is due to aggregation stress [21,50]. In these studies, we observed that larger spheroids had elevated caspase levels, yet there was no hypoxic core and they exhibited decreased packing density, which probably decreased aggregation stress. Annexin V, an early to intermediate marker of apoptosis, was not detected in these spheroids. Thus, cellular apoptosis appears to be a function of neither oxygen tension nor aggregation stress, suggesting an independent mediator in three-dimensional aggregates that warrants further investigation.

We observed decreased glucose consumption with increasing spheroid size, as well as reductions in both intracellular glucose and glucose-6-phosphate, yet we detected no change in glucose metabolism as revealed through the lactate–glucose ratio. Reduced glucose consumption yet maintenance of the lactate–glucose ratio suggests impaired glucose uptake as a function of spheroid size. Whether spheroid diameter regulates expression and/or activity of glucose transporters, perhaps through AMP kinase whose activation is regulated by glucose bioavailability, presents as an intriguing possibility. Previous results in two-dimensional adherent MSCs reveal distinct

metabolic profiles across species [23]. Similarly, MSCs from different donors within a species demonstrate variable lactate–glucose ratios, indicating metabolic heterogeneity [51]. By contrast, we found no difference in the lactate–glucose ratio in spheroids as a function of spheroid size or donor. The metabolic pathways used by MSC spheroids to process glucose and glucose-6-phosphate remain to be defined. That the lactate–glucose ratio decreases with greater cell number per spheroid suggests that glucose is fully oxidized to carbon dioxide by the tricarboxylic acid (TCA) cycle. Alternately, glucose can be diverted to anabolic pathways (pentose phosphate pathway for generation of NADPH for reductive biosynthesis or the formation of ribose-5-phosphate for nucleotide synthesis). Although no other studies have yet examined the bioenergetics of MSC spheroids, work by Liu *et al*. [52] revealed that seeding density influences cellular metabolism. MSCs cultured at low plating density relied upon aerobic glycolysis for ATP production, with reduced coupling of glycolysis to the TCA cycle, and greater activity of the pentose phosphate pathway than cells cultured at higher density [52]. Whether these results translate to three-dimensional culture within spheroids requires greater investigation, but these data suggest that spheroids of varying cell size may have different capacity for the reduction of reactive oxygen species that form upon transplantation into a low-oxygen microenvironment.

One possible mechanism for reduced glucose uptake and cell survival with increasing spheroid size is the decrease in available integrin binding sites due to reduced protein content. While the exact mechanism has yet to be elucidated, the simplified model of spheroid formation involves cell–cell contact, cadherin accumulation, ECM deposition, integrin binding and spheroid compaction [31]. However, as the MSC spheroids adjusted their packing density to allow for the transport of oxygen and nutrients, this came at the expense of ECM deposition and available integrin sites for cell adhesion. Cell-derived matrix enhances cell survival and function [53,54], and MSC spheroid formation can enhance the production of ECM proteins such as laminin, elastin, type 1 collagen and fibronectin [31,55,56]. Furthermore, we recently demonstrated that MSC spheroids containing 15 000 cells per spheroid deposit a collagen-rich ECM, and that the MSCs' integrin–ECM interactions drive cell fate [57]. Therefore, the capacity of spheroid formation to enhance MSC function is at least partially mediated by cell–ECM interactions, and these cell–ECM interactions decreased with increasing spheroid size. This, in turn, may have led to a decrease in cellular metabolism and increased cell apoptosis.

Overall, the discovery that spheroids composed of up to 60 000 MSCs did not exhibit a hypoxic core increases their potential for clinical translation. The ability to form large, viable tissue constructs represents a significant challenge to the field of tissue engineering. As MSC spheroids adapt their packing density and thus do not exhibit necrosis, they represent promising building blocks for the emerging field of bio-printing [58]. MSCs form symbiotic relationships with a myriad of other cell types and could be applied to a variety of different tissues.

Authors' contributions. K.C.M. performed conception and design, financial support, collection and/or assembly of data, data analysis and interpretation and manuscript writing. B.P.H. performed collection and/or assembly of data, data analysis and interpretation and manuscript writing. S.B.-B., D.Z. and J.Y. performed collection and/or assembly of data. D.C.G. designed data analysis and interpretation and manuscript writing. J.K.L. performed conception and design, financial support, data analysis and interpretation, manuscript writing and final approval of the manuscript.

Competing interests. We declare we have no competing interests.

Funding. Research reported in this publication was supported by the National Institute of Dental and Craniofacial Research of the National Institutes of Health under award no. R01-DE025475 (J.K.L.). K.C.M. was supported by an American Heart Association Western States Affiliate Predoctoral Fellowship (15PRE21920010).

Acknowledgements. We thank Dr Volkmar Heinrich and Mr Marco Lee for their assistance in measuring the oxygen tension profiles within the MSC spheroids.

Disclaimer. The content is solely the responsibility of the authors and does not necessarily represent the official views of the National Institutes of Health. The funders had no role in study design, data collection and analysis, decision to publish, or preparation of the manuscript.

References

1. Murphy MB, Moncivais K, Caplan AI. 2013 Mesenchymal stem cells: environmentally responsive therapeutics for regenerative medicine. *Exp. Mol. Med.* **45**, e54. (doi:10.1038/emm.2013.94)
2. Hill E, Boontheekul T, Mooney DJ. 2006 Regulating activation of transplanted cells controls tissue regeneration. *Proc. Natl. Acad. Sci. USA* **103**, 2494–2499. (doi:10.1073/pnas.0506004103).
3. Assmus B *et al.* 2006 Transcoronary transplantation of progenitor cells after myocardial infarction. *N. Engl. J. Med.* **355**, 1222–1232. (doi:10.1056/NEJMoa051779)
4. Bates RC, Edwards NS, Yates JD. 2000 Spheroids and cell survival. *Crit. Rev. Oncol. Hematol.* **36**, 61–74. (doi:10.1016/S1040-8428(00)00077-9)
5. Wang CC, Chen CH, Hwang SM, Lin WW, Huang CH, Lee WY, Chang Y, Sung HW. 2009 Spherically symmetric mesenchymal stromal cell bodies inherent with endogenous extracellular matrices for cellular cardiomyoplasty. *Stem Cells* **27**, 724–732. (doi:10.1634/stemcells.2008-0944)
6. Murphy KC, Fang SY, Leach JK. 2014 Human mesenchymal stem cell spheroids in fibrin hydrogels exhibit improved cell survival and potential for bone healing. *Cell Tissue Res.* **357**, 91–99. (doi:10.1007/s00441-014-1830-z)
7. Cesarz Z, Tamama K. 2016 Spheroid culture of mesenchymal stem cells. *Stem Cells Int.* **2016**, 9176357. (doi:10.1155/2016/9176357)
8. Bhang SH, Lee S, Shin JY, Lee TJ, Kim BS. 2012 Transplantation of cord blood mesenchymal stem cells as spheroids enhances vascularization. *Tissue Eng. Part A* **18**, 2138–2147. (doi:10.1089/ten.TEA.2011.0640)
9. Ho SS, Murphy KC, Binder BY, Vissers CB, Leach JK. 2016 Increased survival and function of mesenchymal stem cell spheroids entrapped in instructive alginate hydrogels. *Stem Cells Transl. Med.* **5**, 773–781. (doi:10.5966/sctm.2015-0211)
10. Korff T, Augustin HG. 1998 Integration of endothelial cells in multicellular spheroids prevents apoptosis and induces differentiation. *J. Cell Biol.* **143**, 1341–1352. (doi:10.1083/jcb.143.5.1341)
11. Curcio E, Salerno S, Barbieri G, De Bartolo L, Drioli E, Bader A. 2007 Mass transfer and metabolic reactions in hepatocyte spheroids cultured in rotating wall gas-permeable membrane system. *Biomaterials* **28**, 5487–5497. (doi:10.1016/j.biomaterials.2007.08.033)
12. Franko AJ, Sutherland RM. 1979 Oxygen diffusion distance and development of necrosis in multicell spheroids. *Radiat. Res.* **79**, 439–453. (doi:10.2307/3575173)
13. Mueller-Klieser W. 1984 Method for the determination of oxygen consumption rates and diffusion coefficients in multicellular spheroids.

Biophys. J. **46**, 343–348. (doi:10.1016/S0006-3495(84)84030-8)

14. Chen B, Longtine MS, Nelson DM. 2013 Pericellular oxygen concentration of cultured primary human trophoblasts. *Placenta* **34**, 106–109. (doi:10.1016/j.placenta.2012.11.011)
15. Langan LM, Dodd NJ, Owen SF, Purcell WM, Jackson SK, Jha AN. 2016 Direct measurements of oxygen gradients in spheroid culture system using electron parametric resonance oximetry. *PLoS ONE* **11**, e0149492. (doi:10.1371/journal.pone.0149492)
16. Malda J, Rouwkema J, Martens DE, Le Comte EP, Kooy FK, Tramper J, van Blitterswijk CA, Riesle J. 2004 Oxygen gradients in tissue-engineered PEGT/PBT cartilaginous constructs: measurement and modeling. *Biotechnol. Bioeng.* **86**, 9–18. (doi:10.1002/bit.20038)
17. Grimes DR, Kelly C, Bloch K, Partridge M. 2014 A method for estimating the oxygen consumption rate in multicellular tumour spheroids. *J. R. Soc. Interface* **11**, 20131124. (doi:10.1098/rsif.2013.1124)
18. Wagner BA, Venkataraman S, Buettner GR. 2011 The rate of oxygen utilization by cells. *Free Radic. Biol. Med.* **51**, 700–712. (doi:10.1016/j.freeradbiomed.2011.05.024)
19. Grantab R, Sivananthan S, Tannock IF. 2006 The penetration of anticancer drugs through tumor tissue as a function of cellular adhesion and packing density of tumor cells. *Cancer Res.* **66**, 1033–1039. (doi:10.1158/0008-5472.CAN-05-3077)
20. Wenger A, Stahl A, Weber H, Finkenzeller G, Augustin HG, Stark GB, Kneser U. 2004 Modulation of *in vitro* angiogenesis in a three-dimensional spheroidal coculture model for bone tissue engineering. *Tissue Eng.* **10**, 1536–1547. (doi:10.1089/ten.2004.10.1536)
21. Bartosh TJ, Ylostalo JH, Mohammadipoor A, Bazhanov N, Coble K, Claypool K, Lee RH, Choi H, Prockop DJ. 2010 Aggregation of human mesenchymal stromal cells (MSCs) into 3D spheroids enhances their antiinflammatory properties. *Proc. Natl Acad. Sci. USA* **107**, 13 724–13 729. (doi:10.1073/pnas.1008117107)
22. Ge J, Guo L, Wang S, Zhang Y, Cai T, Zhao RC, Wu Y. 2014 The size of mesenchymal stem cells is a significant cause of vascular obstructions and stroke. *Stem Cell Rev.* **10**, 295–303. (doi:10.1007/s12015-013-9492-x)
23. Schop D, Janssen FW, van Rijn LD, Fernandes H, Bloem RM, de Bruijn JD, van Dijkhuizen-Radersma R. 2009 Growth, metabolism, and growth inhibitors of mesenchymal stem cells. *Tissue Eng. Part A* **15**, 1877–1886. (doi:10.1089/ten.tea.2008.0345)
24. Pattappa G, Heywood HK, de Bruijn JD, Lee DA. 2011 The metabolism of human mesenchymal stem cells during proliferation and differentiation. *J. Cell Phys.* **226**, 2562–2570. (doi:10.1002/jcp.22605)
25. Verhoven B, Schlegel RA, Williamson P. 1995 Mechanisms of phosphatidylserine exposure, a phagocyte recognition signal, on apoptotic T lymphocytes. *J. Exp. Med.* **182**, 1597–1601. (doi:10.1084/jem.182.5.1597)
26. Vermes I, Haanen C, Steffensnakken H, Reutelingsperger C. 1995 A novel assay for apoptosis—flow cytometric detection of phosphatidylserine expression on early apoptotic cells using fluorescein-labeled Annexin-V. *J. Immunol. Methods* **184**, 39–51. (doi:10.1016/0022-1759(95)00072-I)
27. Chae HJ, Kang JS, Byun JO, Han KS, Kim DU, Oh SM, Kim HM, Chae SW, Kim HR. 2000 Molecular mechanism of staurosporine-induced apoptosis in osteoblasts. *Pharmacol. Res.* **42**, 373–381. (doi:10.1006/phrs.2000.0700)
28. Brown DA, MacLellan WR, Laks H, Dunn JC, Wu BM, Beygui RE. 2007 Analysis of oxygen transport in a diffusion-limited model of engineered heart tissue. *Biotechnol. Bioeng.* **97**, 962–975. (doi:10.1002/bit.21295)
29. Anada T, Fukuda J, Sai Y, Suzuki O. 2012 An oxygen-permeable spheroid culture system for the prevention of central hypoxia and necrosis of spheroids. *Biomaterials* **33**, 8430–8441. (doi:10.1016/j.biomaterials.2012.08.040)
30. Achilli TM, Meyer J, Morgan JR. 2012 Advances in the formation, use and understanding of multi-cellular spheroids. *Expert Opin. Biol. Ther.* **12**, 1347–1360. (doi:10.1517/14712598.2012.707181)
31. Sart S, Tsai AC, Li Y, Ma T. 2014 Three-dimensional aggregates of mesenchymal stem cells: cellular mechanisms, biological properties, and applications. *Tissue Eng. Part B Rev.* **20**, 365–380. (doi:10.1089/ten.TEB.2013.0537)
32. Santos JM *et al.* 2015 Three-dimensional spheroid cell culture of umbilical cord tissue-derived mesenchymal stromal cells leads to enhanced paracrine induction of wound healing. *Stem Cell Res. Ther.* **6**, 90. (doi:10.1186/s13287-015-0082-5)
33. Kim J, Ma T. 2013 Endogenous extracellular matrices enhance human mesenchymal stem cell aggregate formation and survival. *Biotechnol. Prog.* **29**, 441–451. (doi:10.1002/btpr.1686)
34. Moreira JL, Alves PM, Aunins JG, Carrondo MJ. 1995 Hydrodynamic effects on BHK cells grown as suspended natural aggregates. *Biotechnol. Bioeng.* **46**, 351–360. (doi:10.1002/bit.260460408)
35. Michieli P. 2009 Hypoxia, angiogenesis and cancer therapy: to breathe or not to breathe? *Cell Cycle* **8**, 3291–3296. (doi:10.4161/cc.8.20.9741)
36. Martinez I, Nedredal GI, Oie CI, Warren A, Johansen O, Le Couteur DG, Smedsrod B. 2008 The influence of oxygen tension on the structure and function of isolated liver sinusoidal endothelial cells. *Comp. Hepatol.* **7**, 4. (doi:10.1186/1476-5926-7-4)
37. Mohyeldin A, Garzon-Muvdi T, Quinones-Hinojosa A. 2010 Oxygen in stem cell biology: a critical component of the stem cell niche. *Cell Stem Cell* **7**, 150–161. (doi:10.1016/j.stem.2010.07.007)
38. Tatum JL *et al.* 2006 Hypoxia: importance in tumor biology, noninvasive measurement by imaging, and value of its measurement in the management of cancer therapy. *Int. J. Radiat. Biol.* **82**, 699–757. (doi:10.1080/09553000601002324)
39. Santini MT, Rainaldi G. 1999 Three-dimensional spheroid model in tumor biology. *Pathobiology* **67**, 148–157. (doi:10.1159/000028065)
40. Zhang Q, Nguyen AL, Shi S, Hill C, Wilder-Smith P, Krasieva TB, Le AD. 2012 Three-dimensional spheroid culture of human gingiva-derived mesenchymal stem cells enhances mitigation of chemotherapy-induced oral mucositis. *Stem Cells Dev.* **21**, 937–947. (doi:10.1089/scd.2011.0252)
41. Baraniak PR, McDevitt TC. 2012 Scaffold-free culture of mesenchymal stem cell spheroids in suspension preserves multilineage potential. *Cell Tissue Res.* **347**, 701–711. (doi:10.1007/s00441-011-1215-5)
42. Kelm JM, Breitbach M, Fischer G, Odermatt B, Agarkova I, Fleischmann BK, Hoerstrup SP. 2012 3D microtissue formation of undifferentiated bone marrow mesenchymal stem cells leads to elevated apoptosis. *Tissue Eng. Part A* **18**, 692–702. (doi:10.1089/ten.TEA.2011.0281)
43. Potapova IA, Gaudette GR, Brink PR, Robinson RB, Rosen MR, Cohen IS, Doronin SV. 2007 Mesenchymal stem cells support migration, extracellular matrix invasion, proliferation, and survival of endothelial cells *in vitro*. *Stem Cells* **25**, 1761–1768. (doi:10.1634/stemcells.2007-0022)
44. Walenta S, Bredel A, Karbach U, Kunz L, Vollrath L, Mueller-Klieser W. 1989 Interrelationship among morphology, metabolism, and proliferation of tumor cells in monolayer and spheroid culture. *Adv. Exp. Med. Biol.* **248**, 847–853. (doi:10.1007/978-1-4684-5643-1_96)
45. Freyer JP, Sutherland RM. 1986 Regulation of growth saturation and development of necrosis in EMT6/Ro multicellular spheroids by the glucose and oxygen supply. *Cancer Res.* **46**, 3504–3512.
46. Freyer JP, Tustanoff E, Franko AJ, Sutherland RM. 1984 In situ oxygen consumption rates of cells in V-79 multicellular spheroids during growth. *J. Cell Phys.* **118**, 53–61. (doi:10.1002/jcp.1041180111)
47. Tsai AC, Liu Y, Yuan X, Ma T. 2015 Compaction, fusion, and functional activation of three-dimensional human mesenchymal stem cell aggregate. *Tissue Eng. Part A* **21**, 1705–1719. (doi:10.1089/ten.TEA.2014.0314)
48. Wang W, Itaka K, Ohba S, Nishiyama N, Chung UI, Yamasaki Y, Kataoka K. 2009 3D spheroid culture system on micropatterned substrates for improved differentiation efficiency of multipotent mesenchymal stem cells. *Biomaterials* **30**, 2705–2715. (doi:10.1016/j.biomaterials.2009.01.030)
49. Frith JE, Thomson B, Genever PG. 2010 Dynamic three-dimensional culture methods enhance mesenchymal stem cell properties and increase therapeutic potential. *Tissue Eng. Part C Methods* **16**, 735–749. (doi:10.1089/ten.TEC.2009.0432)
50. Ylostalo JH, Bartosh TJ, Coble K, Prockop DJ. 2012 Human mesenchymal stem/stromal cells cultured as spheroids are self-activated to produce prostaglandin E2 that directs stimulated macrophages into an anti-inflammatory phenotype. *Stem Cells* **30**, 2283–2296. (doi:10.1002/stem.1191)
51. Higuera G, Schop D, Janssen F, van Dijkhuizen-Radersma R, van Boxtel T, van Blitterswijk CA. 2009 Quantifying *in vitro* growth and metabolism kinetics of human mesenchymal

stem cells using a mathematical model. *Tissue Eng. Part A* **15**, 2653–2663. (doi:10.1089/ten.TEA.2008.0328)

52. Liu Y, Munoz N, Bunnell BA, Logan TM, Ma T. 2015 Density-dependent metabolic heterogeneity in human mesenchymal stem cells. *Stem Cells* **33**, 3368–3381. (doi:10.1002/stem.2097)
53. Kollmer M, Keskar V, Hauk TG, Collins JM, Russell B, Gemeinhart RA. 2012 Stem cell-derived extracellular matrix enables survival and multilineage differentiation within superporous hydrogels. *Biomacromolecules* **13**, 963–973. (doi:10.1021/bm300332w)
54. Hoch AI, Mittal V, Mitra D, Vollmer N, Zikry CA, Leach JK. 2016 Cell-secreted matrices perpetuate the bone-forming phenotype of differentiated mesenchymal stem cells. *Biomaterials* **74**, 178–187. (doi:10.1016/j.biomaterials.2015.10.003)
55. Shearier E, Xing Q, Qian Z, Zhao F. 2016 Physiologically low oxygen enhances biomolecule production and stemness of mesenchymal stem cell spheroids. *Tissue Eng. Part C Methods* **22**, 360–369. (doi:10.1089/ten.TEC.2015.0465)
56. Amos PJ, Kapur SK, Stapor PC, Shang H, Bekiranov S, Khurgel M, Rodeheaver GT, Peirce SM, Katz AJ. 2010 Human adipose-derived stromal cells accelerate diabetic wound healing: impact of cell formulation and delivery. *Tissue Eng. Part A* **16**, 1595–1606. (doi:10.1089/ten.TEA.2009.0616)
57. Murphy KC, Hoch AI, Harvestine JN, Zhou D, Leach JK. 2016 Mesenchymal stem cell spheroids retain osteogenic phenotype through $\alpha 2\beta 1$ signaling. *Stem Cells Transl. Med.* **5**, 1229–1237. (doi:10.5966/sctm.2015-0412)
58. Blakely AM, Manning KL, Tripathi A, Morgan JR. 2015 Bio-pick, place, and perfuse: a new instrument for three-dimensional tissue engineering. *Tissue Eng. Part C Methods* **21**, 737–746. (doi:10.1089/ten.TEC.2014.0439)